Study of differential operators in the context of the semi-analytical wall boundary conditions

Study of differential operators in the context of the semi-analytical wall boundary conditions

Arno Mayrhofer, Benedict D. Rogers
School of Mechanical, Aerospace and Civil Engineering
University of Manchester
Manchester, United Kingdom
arno.m@gmx.at

Damien Violeau, Martin Ferrand
Laboratoire National d'Hydraulique et d'Environnement
Électricité de France R&D
Chatou, France

***Abstract*—In this paper the semi-analytical wall boundary conditions by Ferrand et al. [1] are investigated theoretically by looking at the property of skew-adjointness in a continuous setting. As stabilizing procedure a volume diffusion term [2] is used and a new interpretation for it is given in the Reynolds averaged context. Additonally, a correction term for external forces is presented. The final theoretical contribution concerns arbitrary order Robin boundary conditions. The theoretical constructs are then investigated in various confined and free-surface flows. The issue of convergence is illustrated in the case of Poiseuille flow, the external force correction terms in the volume diffusion term and the boundary conditions are demonstrated via still water simulations. Finally, a standing wave and a dam-break over a wedge is simulated and quantitative comparisons are given. The paper is concluded by highlighting the difficulties associated with the extension to three dimensions as well as giving an insight into the current developments.**

I. Introduction

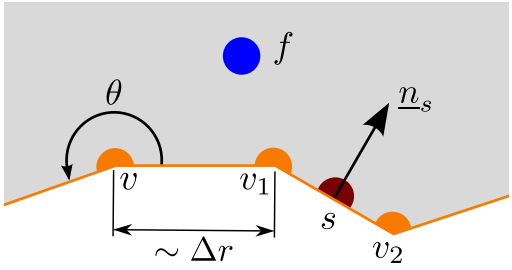

Fig. 1. The different types of elements.

Semi-analytical wall boundary conditions for arbitrary boundaries in SPH were introduced by Ferrand *et al.* in [1], [3], [4]. We first recall the main principles of this method. The key idea was to use an analytical kernel correction factor γ given by

$$\gamma_a = \int_\Omega w_{ab} \mathrm{d}\underline{r}_b. \tag{1}$$

The boundary conditions are implemented by using the sets of elements described in Table I. The fluid is discretized using particles. The boundary is split into line segments of length approximately Δr. These segments are called boundary elements and are located between two vertex particles as shown in Fig. 1.

Set	Description
$\mathcal{P}$	All particles
$\mathcal{V}$	Particles on boundary (vertex particles)
$\mathcal{F}$	Particles inside the fluid domain
$\mathcal{S}$	Boundary segments

TABLE I
Overview of elements.

In the following differential operators will be written in bold (e.g. **Div**). Vectors and matrices will be written as $\underline{B}$ and $\underline{\underline{M}}$ respectively. The general SPH approximation for a scalar f at position a is given by

$$[f]_a = \frac{1}{\gamma_a} \sum_{b \in \mathcal{P}} V_b f_b w_{ab}, \tag{2}$$

where V is the volume, $\mathcal{P}$ the set of all particles and w the SPH kernel. In order to obtain the analytical value for γ, a governing equation is used, given by

$$\frac{\mathrm{d}\gamma_a}{\mathrm{d}t} = \underline{v}_a^r \cdot \underline{\nabla}\gamma_a, \tag{3}$$

where $\underline{v}^r$ is the velocity relative to the wall. Ferrand *et al.* [3] derived an analytical expression for $\underline{\nabla}\gamma_a$ in 2-D for the Wendland kernel. Without loss of generality this kernel will be used throughout this paper. The other key idea is to rigorously derive the differential operators without neglecting boundary terms coming from the integration by parts. For the SPH approximation as given by Eq. (2) Ferrand *et al.* proposed the following SPH approximation for the divergence of a vector field $\underline{B}$

$$\mathbf{Div}_a^{\gamma,F}(\underline{B}) := -\frac{1}{\gamma_a \rho_a} \sum_{b \in \mathcal{P}} m_b \underline{B}_{ab} \cdot \underline{\nabla}_a w_{ab} + \frac{1}{\gamma_a} \sum_{s \in \mathcal{S}} \underline{B}_{as} \cdot \underline{\nabla}\gamma_{as}, \tag{4}$$

where the superscript F stands for "Ferrand" and $\underline{B}_{ab} = \underline{B}_a - \underline{B}_b$. Following the same paper, the gradient of a scalar field f

is given by

$$\mathbf{Grad}_a^{\gamma,F}(f) = \frac{\rho_a}{\gamma_a}\sum_{b\in\mathcal{P}} m_b\left(\frac{f_a}{\rho_a^2}+\frac{f_b}{\rho_b^2}\right)\underline{\nabla} w_{ab} - \frac{\rho_a}{\gamma_a}\sum_{s\in\mathcal{S}}\left(\frac{f_a}{\rho_a^2}+\frac{f_s}{\rho_s^2}\right)\rho_s\underline{\nabla}\gamma_{as}, \quad (5)$$

where

$$\underline{\nabla}\gamma_{as} = \int_s w_{ab}\underline{n}_b \mathrm{d}\underline{r}_b, \quad (6)$$

is the integral of the kernel over a segment s. Note that this integral is known analytically.
Still following [1], in order to impose Neumann boundary conditions at the wall for a scalar f the values from the fluid are extrapolated to a vertex particle v via

$$f_v = \frac{1}{\alpha_v}\sum_{b\in\mathcal{F}} V_b\, f_b\, w_{vb}, \quad (7)$$

where

$$\alpha_v := \sum_{b\in\mathcal{F}} V_b\, w_{bv}. \quad (8)$$

Finally, the values for the boundary elements are given as arithmetic mean of the associated vertex particles. In the following the above considerations and tools will be modified and improved.

II. Skew-adjoint operators

In this section the focus will be on the property of skew-adjointness of the two arbitrary operators **Grad** and **Div**. In the continuous case the following holds

$$\underbrace{\langle\underline{\nabla} f, \underline{B}\rangle + \langle f, \underline{\nabla}\cdot\underline{B}\rangle}_{=:(*)} = \int_{\partial\Omega} f(\underline{r})\,\underline{B}(\underline{r})\cdot\underline{n}(\underline{r})\mathrm{d}\underline{r}, \quad (9)$$

where $\langle\rangle$ are the respective L^2 scalar products. If $f = p$ and $\underline{B} = \underline{v}$, the pressure and velocity respectively which solve the Navier-Stokes equations, then the right-hand side is equal to zero. This is due to $p = 0$ at a free-surface and $\underline{v}\cdot\underline{n} = 0$ at a solid wall. If the right-hand side is equal to zero the system conserves energy. Thus the SPH operators should ideally adhere to this property.
The investigation will commence by considering basic continuous SPH operators without boundary terms, i.e. using integrals instead of discrete sums and assuming that no boundaries are present. The operators under investigation are given by

$$\mathbf{Grad}_a^b(f) := \int_\Omega f_b\underline{\nabla}_a w_{ab}\mathrm{d}\underline{r}_b \quad (10)$$

$$\mathbf{Div}_a^b(\underline{B}) := \int_\Omega \underline{B}_b\cdot\underline{\nabla}_a w_{ab}\mathrm{d}\underline{r}_b, \quad (11)$$

where the superscript b stands for "basic". The left-hand side of Eq. (9) is then given by

$$(*) = \int_\Omega\int_\Omega (f_b\,\underline{\nabla}_a w_{ab}\cdot\underline{B}_a + f_a\,\underline{B}_b\cdot\underline{\nabla}_a w_{ab})\,\mathrm{d}\underline{r}_b\mathrm{d}\underline{r}_a. \quad (12)$$

Swapping the labels a, b in the second term yields

$$(*) = \int_\Omega\int_\Omega (f_b\,\underline{B}_a\cdot\underline{\nabla}_a w_{ab} + f_b\,\underline{B}_a\cdot\underline{\nabla}_a w_{ab})\,\mathrm{d}\underline{r}_b\mathrm{d}\underline{r}_a. \quad (13)$$

Using the kernel asymmetry, i.e. $\underline{\nabla}_a w_{ab} = -\underline{\nabla}_a w_{ab}$ finally shows that $(*) = 0$, i.e. that $\mathbf{Grad}^b$ and $\mathbf{Div}^b$ are skew-adjoint. Note that this property also holds true in the discrete case, where the integrals are replaced by sums.
The symmetrised operators

$$\mathbf{Grad}_a^{bs}(f) := \int_\Omega (f_b + f_a)\underline{\nabla}_a w_{ab}\mathrm{d}\underline{r}_b \quad (14)$$

$$\mathbf{Div}_a^{bs}(\underline{B}) := \int_\Omega (\underline{B}_b - \underline{B}_a)\cdot\underline{\nabla}_a w_{ab}\mathrm{d}\underline{r}_b, \quad (15)$$

are skew-adjoint if the newly added terms have opposing signs. The proof, which will be omitted, can be found e.g. in [5]. As in the previous case it holds true in the discrete case as well. When dropping the assumption of no boundaries the calculations are no longer as simple. Firstly, observe that

$$\frac{1}{\gamma_a}\int_\Omega w_{ab}\mathrm{d}\underline{r}_b = 1. \quad (16)$$

Note, that the renormalization is necessary to obtain the correct value on the boundaries. The operators of interest in the following are given in continuous form by

$$\mathbf{Grad}_a^\gamma(f) := \frac{1}{\gamma_a}\int_\Omega (f_b + f_a)\underline{\nabla}_a w_{ab}\mathrm{d}\underline{r}_b - \frac{1}{\gamma_a}\int_{\partial\Omega}(f_b + f_a)\underline{n}_b w_{ab}\mathrm{d}\underline{r}_b, \quad (17)$$

$$\mathbf{Div}_a^\gamma(\underline{B}) := \frac{1}{\gamma_a}\int_\Omega (\underline{B}_b - \underline{B}_a)\cdot\underline{\nabla}_a w_{ab}\mathrm{d}\underline{r}_b - \frac{1}{\gamma_a}\int_{\partial\Omega}(\underline{B}_b - \underline{B}_a)\cdot\underline{n}_b w_{ab}\mathrm{d}\underline{r}_b, \quad (18)$$

where the superscript γ indicates the renormalization. Initially the volumic part of Eq. (9) will be investigated.

$$(*)_v = \int_\Omega\int_\Omega \frac{1}{\gamma_a}[(f_a + f_b)\underline{B}_a - f_a(\underline{B}_a - \underline{B}_b)]\cdot\underline{\nabla}_a w_{ab}\mathrm{d}\underline{r}_b\mathrm{d}\underline{r}_a \quad (19)$$

$$= \int_\Omega\int_\Omega \frac{1}{\gamma_a}[f_b\underline{B}_a + f_a\underline{B}_b]\cdot\underline{\nabla}_a w_{ab}\mathrm{d}\underline{r}_b\mathrm{d}\underline{r}_a \quad (20)$$

$$= \int_\Omega\int_\Omega f_b\underline{B}_a\cdot\left[\frac{\underline{\nabla}_a w_{ab}}{\gamma_a} + \frac{\underline{\nabla}_a w_{ab}}{\gamma_b}\right]\mathrm{d}\underline{r}_b\mathrm{d}\underline{r}_a. \quad (21)$$

The boundary part of Eq. (9) can be reformulated to

$$(*)_b = \int_\Omega\int_{\partial\Omega}\frac{1}{\gamma_a}[-(f_a + f_b)\underline{B}_a + f_a(\underline{B}_a - \underline{B}_b)]\cdot\underline{n}_b w_{ab}\mathrm{d}\underline{r}_b\mathrm{d}\underline{r}_a \quad (22)$$

$$= \int_\Omega\int_{\partial\Omega}\frac{1}{\gamma_a}[-f_b\underline{B}_a - f_a\underline{B}_b]\cdot\underline{n}_b w_{ab}\mathrm{d}\underline{r}_b\mathrm{d}\underline{r}_a. \quad (23)$$

Combining the volumic $(*)_v$ and the boundary term $(*)_b$, as well as applying Stokes' Theorem and integration by parts

yields

$$(*) = \int_\Omega \frac{\underline{B}_a}{\gamma_a} \cdot \int_\Omega \underline{\nabla}_b(f) w_{ab} \mathrm{d}\underline{r}_b \mathrm{d}\underline{r}_a \quad (24)$$
$$+ \int_\Omega \frac{f_b}{\gamma_b} \int_\Omega (\underline{\nabla}_a \cdot \underline{B}) w_{ab} \mathrm{d}\underline{r}_a \mathrm{d}\underline{r}_b$$
$$= \int_\Omega \underline{\nabla}_a \cdot (f\underline{B}) \frac{1}{\gamma_a} \int_\Omega w_{ab} \mathrm{d}\underline{r}_b \mathrm{d}\underline{r}_a. \quad (25)$$

Eq. (24) is not surprising as it shows just the definition of the SPH approximation of differential operators. However, it demonstrates the tools required for deriving the same result for discrete operators. Next, Eq. (25) becomes, with the use of Eq. (16)

$$(*) = \int_\Omega \underline{\nabla}_a \cdot (f\underline{B}) \mathrm{d}\underline{r}_a \quad (26)$$
$$= \int_{\partial\Omega} f_a \underline{B}_a \cdot \underline{n}_a \mathrm{d}\underline{r}_a. \quad (27)$$

This is equivalent to Eq. (9) showing the skew-adjoint property for SPH continuous operators with boundary terms in case of the correct imposition of the boundary conditions. Note that it is essential for this result that the operators are renormalized with γ. The gradient as derived by Kulasegaram *et al.* in [6] cannot fulfill the skew-adjoint principle as it contains one γ term inside the sum.

The calculation shown above could have been made much shorter, when only considering continuous operators. However, the reason for explicitly going through this calculation was in order to show the tools necessary for proving the same in the discrete case. It would thus be necessary to have a discrete version of the Stokes' theorem. Additionally, γ should equal to the Sheppard filter, which is not a desired property due to the increased numerical viscosity. The difficulty for a discrete Stokes' theorem comes from the fact that $\underline{\nabla}\gamma$ is calculated analytically along the wall, whereas the volumic integral over $\underline{\nabla}w$ is approximated via a discrete sum.

Inside the fluid ($\gamma = 1$, no boundary terms) the skew-adjoint property is fulfilled in the discrete case as it is equivalent to the basic, symmetrized differential operators (**Div**^{bs}, **Grad**^{bs}). Finally, the discretized forms of Eqs. (17) and (18) are given by

$$\mathbf{Grad}^\gamma_a(f) = \frac{1}{\gamma_a} \sum_{b\in\mathcal{P}} V_b (f_b + f_a) \underline{\nabla}_a w_{ab} \quad (28)$$
$$- \frac{1}{\gamma_a} \sum_{s\in\mathcal{S}} (f_s + f_a) \underline{\nabla}\gamma_{as}$$
$$\mathbf{Div}^\gamma_a(\underline{B}) = \frac{1}{\gamma_a} \sum_{b\in\mathcal{P}} V_b (\underline{B}_b - \underline{B}_a) \cdot \underline{\nabla}_a w_{ab} \quad (29)$$
$$- \frac{1}{\gamma_a} \sum_{s\in\mathcal{S}} (\underline{B}_s - \underline{B}_a) \cdot \underline{\nabla}\gamma_{as}.$$

Note that these operators differ slightly from the ones derived by Ferrand *et al.* given by Eqs. (5) and (4).

III. Volume diffusion term

The volume diffusion term introduced by Ferrari *et al.* in [2] is given by

$$\frac{\mathrm{d}\rho_a}{\mathrm{d}t} = \sum_{b\in\mathcal{P}} V_b \left(\rho_b \underline{v}_{ab} + c_{ab} \frac{\underline{r}_{ab}}{r_{ab}} \rho_{ab} \right) \cdot \underline{\nabla} w_{ab}, \quad (30)$$

where $r_{ab} = \|\underline{r}_{ab}\|$,

$$c_{ab} = \max(c_a, c_b), \quad (31)$$

and

$$c_a = c_0 \sqrt{\left(\frac{\rho_a}{\rho_0}\right)^{\xi-1}}, \quad (32)$$

where ξ is the exponent from the Tait Equation of State, taken to be 7 for water.

In the original paper [2] this term is derived from a Riemann solver perspective. In the following a different interpretation of this term will be given.

A. RANS interpretation

In the context of turbulent flows the continuity equation in the Reynolds averaged context is given by

$$\frac{\overline{\mathrm{d}}\overline{\rho}}{\overline{\mathrm{d}}t} = -\overline{\rho}\underline{\nabla} \cdot \underline{\overline{v}} - \underline{\nabla} \cdot (\overline{\rho' \underline{v}'}), \quad (33)$$

where the primes refer to turbulent fluctuations and the bars the Reynolds averaging. Although this correction is applied to laminar flow where the fluctuating quantities are supposed to be zero, they can be interpreted as numerical fluctuations. The gradient-diffusion hypothesis claims that

$$\overline{\rho' \underline{v}'} = -K \underline{\nabla} \overline{\rho}. \quad (34)$$

Inserting this into the averaged continuity equation yields

$$\frac{\overline{\mathrm{d}}\overline{\rho}}{\overline{\mathrm{d}}t} = -\overline{\rho}\underline{\nabla} \cdot \underline{\overline{v}} + \underline{\nabla} \cdot (K \underline{\nabla} \overline{\rho}). \quad (35)$$

As no fluctuating quantities remain we will neglect the bars in the following. In terms of SPH operators the following is obtained

$$\frac{\mathrm{d}\rho_a}{\mathrm{d}t} = -\rho_a \mathbf{Div}_a(\underline{v}) + \mathbf{Lap}_a(K, \rho), \quad (36)$$

where **Lap** is an SPH discrete operator, here applied to ρ with a diffusion coefficient K. If the model by Morris [7] is used for the discretisation of the **Lap** operator then the full discretisation reads

$$\frac{\mathrm{d}\rho_a}{\mathrm{d}t} = -\rho_a \sum_{b\in\mathcal{P}} V_b \left(\underline{v}_{ba} + (K_a + K_b) \rho_{ab} \frac{\underline{r}_{ab}}{\underline{r}^2_{ab}} \right) \cdot \underline{\nabla}_a w_{ab}. \quad (37)$$

Comparing Eqs. (37) and (30) it can be deduced that

$$c_{ab} = \frac{K_a + K_b}{r_{ab}}. \quad (38)$$

Now having a closer look at c_a, given by (32), shows that

$$c_a = c_0 \left(\frac{\rho_a}{\rho_0}\right)^{\frac{\xi-1}{2}} = \sqrt{\left.\frac{\partial p}{\partial \rho}\right|_a}, \quad (39)$$

so c_a is nothing else than the speed of sound of particle a. Thus K has the dimension m^2/s as it is expected for the turbulent diffusivity term. It is common to write the diffusivity term as

$$K = \frac{\nu_T}{\sigma_T}, \tag{40}$$

where ν_T is the turbulent viscosity and σ_T is the turbulent Prandtl number. Using the mixing length model this can be written as

$$K \approx \frac{1}{\sigma_T} L_m^2 \frac{V}{L}, \tag{41}$$

where V and L are characteristic velocity and length scales respectively and L_m is the mixing length. Defining the Mach number as $Ma = V/c_0$ yields

$$K = \frac{1}{\sigma_T} L_m^2 \frac{c_0\, Ma\, \Delta r}{L \Delta r}. \tag{42}$$

Typically $L_m = L/10$ and $Ma = 1/10$, which yields

$$K = \frac{1}{\sigma_T} \frac{L}{\Delta r} \frac{c_0\, \Delta r}{10^3}. \tag{43}$$

Depending on the resolution K can thus be given as

$$K = c_0\, \Delta r/\alpha, \tag{44}$$

with $\alpha = \mathcal{O}(10)$ or $\alpha = \mathcal{O}(100)$ for high or low resolution respectively. From this and Eq. (38) it can be seen that the correction as proposed by Ferrari *et al.* [2] applies a significantly higher viscosity term than what can be derived from the simple mixing length model. This fact can be of importance when it comes to the use of this correction in the context of Large Eddy Simulation. The turbulent viscosity introduced due to the volume diffusion term can dissipate more than just the numerical noise and thus have an influence on the energy spectrum of the flow.

B. Semi-analytical wall boundary framework

After this interpretation the question arises on how this additional numerical viscosity term can be included in the wall boundary formulation as described above. In order to do so, the flux of the quantity $K\underline{\nabla}\rho$ has to be investigated in normal direction of the wall. As the boundary condition on the density implies $\partial\rho/\partial\underline{n} = 0$ this flux is zero as well. Thus, using the Laplacian of Ferrand [1], [3] and the divergence given by Eq. (29) the continuity equation with volume diffusion term reads

$$\begin{aligned} \frac{\mathrm{d}\rho_a}{\mathrm{d}t} &= -\frac{\rho_a}{\gamma_a} \sum_{b\in\mathcal{P}} V_b \left(\underline{v}_{ba} + \frac{c_{ab}}{\rho_a} \rho_{ab} \frac{\underline{r}_{ab}}{r_{ab}} \right) \cdot \underline{\nabla}_a w_{ab} \\ &\quad + \frac{\rho_a}{\gamma_a} \sum_{s\in\mathcal{S}} \underline{v}_{sa} \cdot \underline{\nabla}\gamma_{as}. \end{aligned} \tag{45}$$

C. Free-surface flows

Using the volume diffusion term in a simulation of still water shows that the term as shown above will not have a zero contribution towards the density equation. In order to compensate for this deficiency the correction can be modified so that it reads

$$\begin{aligned} \frac{\mathrm{d}\rho_a}{\mathrm{d}t} &= \frac{\rho_a}{\gamma_a} \sum_{b\in\mathcal{P}} V_b \left(\underline{v}_{ab} + \frac{c_{ab}}{\rho_a} \varrho_{ab} \frac{\underline{r}_{ab}}{r_{ab}} \right) \cdot \underline{\nabla}_a w_{ab} \\ &\quad - \frac{\rho_a}{\gamma_a} \sum_{s\in\mathcal{S}} \underline{v}_{as} \cdot \underline{\nabla}\gamma_{as}, \end{aligned} \tag{46}$$

where ϱ_{ab} is given by

$$\varrho_{ab} = \left[\frac{\xi}{c_0^2 \rho_0} (p_a - \rho_0 g(z_b - z_a)) + 1 \right]^{\frac{1}{\xi}} \rho_0 - \rho_b, \tag{47}$$

which approximates the difference between the non-hydrostatic densities. The last equation is simply the non-hydrostatic pressure applied to the inverted equation of state.

IV. Arbitrary-order Robin wall boundary conditions

To satisfy von Neumann boundary conditions Ferrand *et al.* [1] showed a first order approximation approach (see Eqs. (7) and (8)). In the following this approach shall be generalized to arbitrary orders of accuracy and to Robin boundary conditions. Such a boundary condition is given by

$$\left(\mu_1 f + \mu_2 \frac{\partial f}{\partial \underline{n}} \right) \Big|_{\partial\Omega} = \mu_3, \tag{48}$$

for an arbitrary scalar field f with given $\mu_1, \mu_2 \neq 0, \mu_3$. In order to impose Neumann boundary conditions μ_1, μ_2 take the values $0, 1$. The above can be rewritten as

$$\frac{\partial f}{\partial \underline{n}} = \frac{\mu_3 - \mu_1 f}{\mu_2}. \tag{49}$$

The key idea is to use a weighted linear least squares approximation of the desired field in direction of the normal $\underline{n}_v$ of a vertex particle v. This implies that the problem is one dimensional. Let n be the desired order of approximation and a polynomial λ shall be defined as

$$\lambda(x) = \sum_{i=2}^{n} \beta_i x^i + \frac{\mu_3 - \mu_1 \beta_1}{\mu_2} x + \beta_1. \tag{50}$$

Note the fact that $\beta_1 = f\big|_{\partial\Omega}$, i.e. β_1 is the value at the wall. The polynomial can also be written as

$$\lambda(x) = \sum_{i=2}^{n} \beta_i x^i + \frac{\mu_3}{\mu_2} x + \beta_1 \left(1 - \frac{\mu_1}{\mu_2} x \right). \tag{51}$$

It represents f in direction of the normal $\underline{n}_v$ with $f_v = \lambda(0)$. For a fluid particle $a \in \mathcal{F}$, the value of λ_a is thus given as $\lambda(\underline{r}_{av} \cdot \underline{n}_v)$ in case no external forces are present. Let $\underline{\underline{X}} \in \mathbb{M}(n, |\mathcal{F}|)$ be defined as

$$\underline{\underline{X}}_{aj} = \begin{cases} 1 - \frac{\mu_1}{\mu_2} (\underline{r}_{av} \cdot \underline{n}_v) & \text{if } j = 1, \\ (\underline{r}_{av} \cdot \underline{n}_v)^j & \text{if } j > 1, \end{cases} \tag{52}$$

where $\underline{y} \in \mathbb{R}^{|\mathcal{F}|}$ is given by

$$y_a = f_a - \frac{\mu_3}{\mu_2} (\underline{r}_{av} \cdot \underline{n}_v). \tag{53}$$

Thus, we are looking for a solution of the over constrained system of linear equations

$$\underline{\underline{X}} \cdot \underline{\beta} = \underline{y}, \tag{54}$$

where $\underline{\beta} = \beta_i$. A common approach to this type of problem is to use the least squares method which can be solved via

$$\underline{\underline{X}}^T \cdot \underline{\underline{X}} \cdot \underline{\beta} = \underline{\underline{X}}^T \cdot \underline{y}. \tag{55}$$

In order to put more weight on particles closer to the vertex particle, the SPH kernel is used to construct a weighted least squares interpolation. To include this into the above let $\underline{\underline{\Lambda}} \in \mathbb{M}(|\mathcal{F}|)$ be defined as

$$\underline{\underline{\Lambda}}_{ab} = \delta_{ab} V_a w_{va}, \tag{56}$$

(there is no summation over indices here). Then the weighted least squares interpolation can be found by solving

$$\underline{\underline{X}}^T \cdot \underline{\underline{\Lambda}} \cdot \underline{\underline{X}} \cdot \underline{\beta} = \underline{\underline{X}}^T \cdot \underline{\underline{\Lambda}} \cdot \underline{y}. \tag{57}$$

Due to the fact that the problem is one dimensional the matrix on the left-hand side is of size $n \times n$ and can be inverted easily. Of interest is $\lambda(0)$ which is nothing else than β_1. Thus finally

$$f_v = \lambda(0) = \beta_1 = ((\underline{\underline{X}}^T \cdot \underline{\underline{\Lambda}} \cdot \underline{\underline{X}})^{-1} \cdot \underline{\underline{X}}^T \cdot \underline{\underline{\Lambda}} \cdot \underline{y})_1. \tag{58}$$

If $n = 1$ the above reduces to the equation shown in Eq. (7) thus showing that this indeed is a generalization. Note that the matrix that needs to be inverted $(\underline{\underline{X}}^T \cdot \underline{\underline{\Lambda}} \cdot \underline{\underline{X}})$ is contained in $\mathbb{M}(n)$ and thus to obtain second-order boundary conditions the inversion of a 2×2 matrix is required in two dimensions. Finally it shall be noted that the matrix is non-degenerate if at least n fluid particles are in the neighbourhood of v and that they have different values of $(\underline{r}_{av} \cdot \underline{n}_v)$.

A. Including external forces

In this section the case $f = p$ (pressure) will be investigated in the presence of gravity. The approach presented above will produce unsatisfactory results at the intersection of free-surface and wall as tangential variations are not neglected. The constraint above reads

$$\lambda_a = \lambda(\underline{r}_{av} \cdot \underline{n}_v) = p_a. \tag{59}$$

In order to neglect tangential variations for external forces, such as gravity the proper constraint is given by

$$\lambda_a = \lambda(\underline{r}_{av} \cdot \underline{n}_v) = p_a - (\underline{r}_{av} - (\underline{r}_{av} \cdot \underline{n}_v)\underline{n}_v) \cdot \underline{g}\rho_0. \tag{60}$$

V. 2-D Simulations

In this section several simulations will be shown, illustrating the theoretical tools presented above. The first flow is the laminar Poiseuille flow which will be utilized for a convergence analysis. Two still water test cases are shown, illustrating the effect of the external force corrections both in the volume diffusion term as well as in the boundary conditions. Finally, two laminar free-surface flows are presented, the standing wave and a dam-break over a wedge for which the force on the left wedge wall is measured and compared to a Volume of Fluid code.

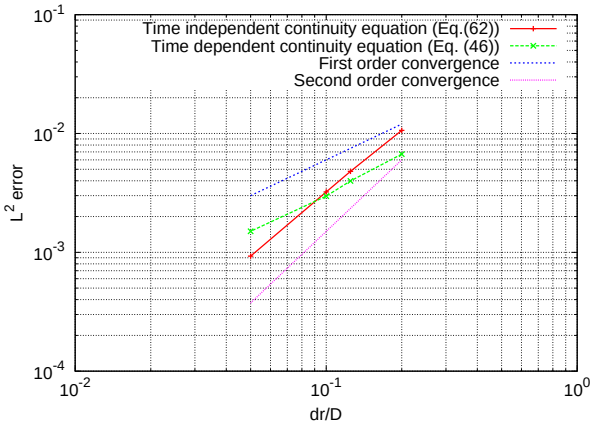

Fig. 2. Convergence study of a laminar channel flow.

A. Poiseuille flow

In this section the periodic laminar Poiseuille flow will be studied. The Reynolds number is equal to 10 and the analytical velocity profile is given by

$$u = 4Re\frac{\nu}{H}\frac{z}{H}(1 - \frac{z}{H}), \tag{61}$$

where H is the height of the channel, ν the kinematic viscosity and Re the Reynolds number. In Fig. 2 the convergence of the SPH method is studied by comparing two different continuity equations. The time-independent continuity equation is given by Ferrand *et al.* [1] as

$$\mathrm{d}(\gamma_a \rho_a) = \sum_{b \in \mathcal{P}} m_b \mathrm{d}(w_{ab}). \tag{62}$$

and the time-dependent one is given by Eq. (46). As can be seen in Fig. 2 the time-independent continuity equation shows second-order convergence, whereas the time-dependent one converges only linearly. The time-step was kept constant as to only measure convergence in space. This discrepancy in convergence order is quite surprising and no explanation of it could be found. It can be ensured that the volume diffusion term (Section III) is not the cause, as without it the convergence rate is the same, although the error is much larger. The SPH simulation of the periodic Poiseuille flow is inherently unstable as shown by Basa *et al.* [8]. Stability in this case refers to the degree of particle disorder. In general the continuity equation with volume diffusion term is significantly more stable than the one without. It is also more stable than the time-independent continuity equation.

B. Still water test cases

In order to demonstrate the proposed modification of the volume diffusion term (Section III), a simulation of still water in a periodic open channel will be presented. In Fig. 3 the position of a fluid particle on the free-surface is plotted over time. The initial density is uniform and thus a slight drop due to the weak compressibility will be expected. The simulation without a volume diffusion correction shows exactly this drop

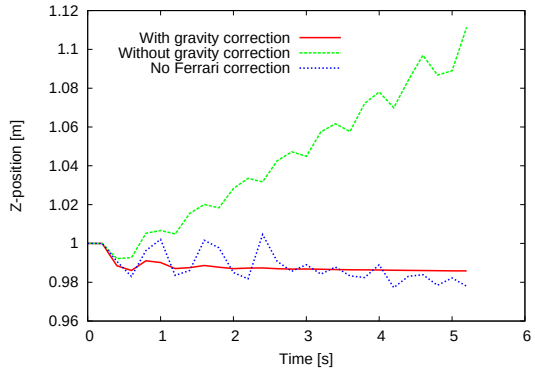

Fig. 3. Impact of the free-surface correction as given by Eq. (46).

including numerical noise. If the volume diffusion term by Ferrari *et al.* [2] is added the free surface will rise, causing the solution to diverge. This is no surprise as the $\rho_a - \rho_b$ term in Eq. (45) is non-zero. Finally, the simulation with the gravity correction (Eq. (46)) again shows the expected drop and the additional damping.

In Fig. 4 the boundary conditions by Ferrand *et al.* given

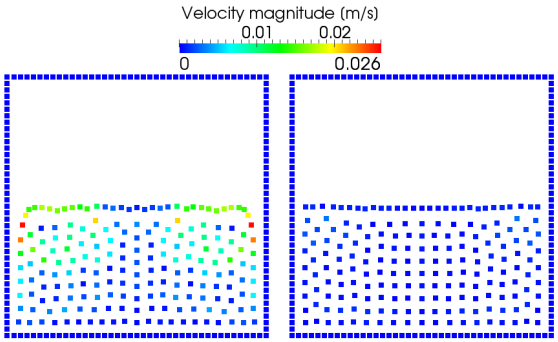

Fig. 4. Impact of the external force correction as given by Eq. (60).

in Eq. (7) are compared to the ones presented in Section IV taking into account Eq. (60) which correctly treats external forces. The original formulation shows an increased pressure of the vertex particles close to the free-surface causing the fluid to be pushed inwards. The novel approach does not exhibit this behaviour and thus the overall velocity after 20 seconds is only a tenth compared to the original formulation. Note that in both cases it can be observed that the two top rows of fluid particles merge and thus the free-surface is constituted of particles with spacing $\Delta r/2$.

C. Standing wave

The next simulation that is shown is from an inviscid standing wave. A few snapshots of this simulation can be seen in Fig. 5. There, the evolution during the 10th period is shown, illustrating the extrema of excitation as well as the intermediate states with flat free-surface and maximum velocity. Due to the inviscid nature of the problem, it is essential to apply an artificial diffusion (Eq. (45)), as without

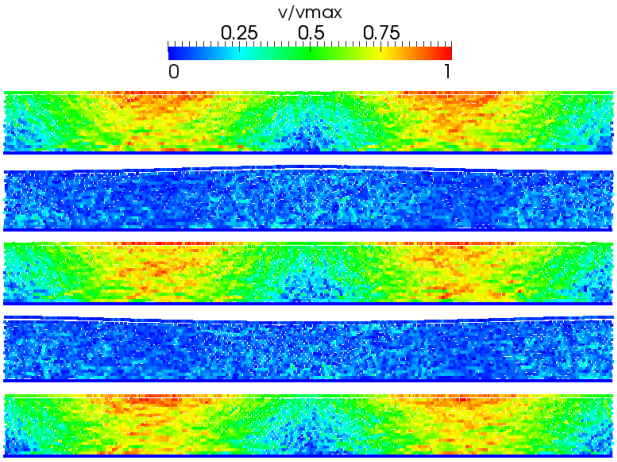

Fig. 5. Time evolution of the standing wave.

it, the simulation would not be stable. The fluid is initially at rest so that the particles can rearrange themselves. This specifically at the free-surface, as already shown in Fig. 4. After that the simulation is started by imposing the analytical velocity profile as given by Dean and Dalrymple [9]. The velocity potential Φ can be written as

$$\Phi = \frac{H_s g}{2\sigma} \frac{\cosh(k\,z)}{\cosh(k\,h)} \cos(k\,x) \sin(\sigma\,t), \tag{63}$$

where $\sigma = g\,k \tanh(k\,h)$ and $k = 2\pi/L$. The pressure distribution reads

$$p = -\rho\,g\,z + \rho\,g \frac{H_s \cosh(k\,z)}{2\cosh(k\,h)} \cos(k\,x) \cos(\sigma\,t). \tag{64}$$

The wave length $L = 10m$, the water depth $h = 10m$ and the wave height $H_s = 0.1m$. The particle spacing Δr is equal to half the wave height H_s. In Fig. 5 it can be seen that the velocity profile exhibits a significant amount of noise. The constant α in front of the volume diffusion term (Eq. (44)) is set to $100/6$. This value is chosen, such that the simulation

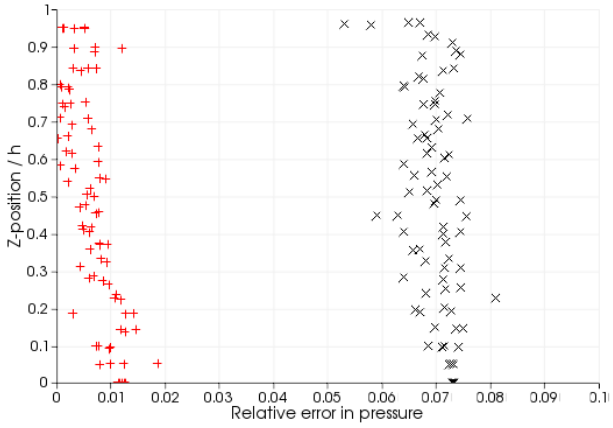

Fig. 6. Error in pressure after 10 periods under crest (black) and trough (red).

keeps stable, while minimizing the diffusion associated with it. Finally, in Fig. 6 the relative error in pressure (when compared to the theory) can be seen under a trough (red pluses) and a crest (black crosses). Note that it was not possible to reproduce the period of the standing wave. Because of that the analytical time was shifted in order to reproduce the plots in Fig. 6. No reason for this shift could be found and it will be part of future investigations.

D. Dam-break over wedge

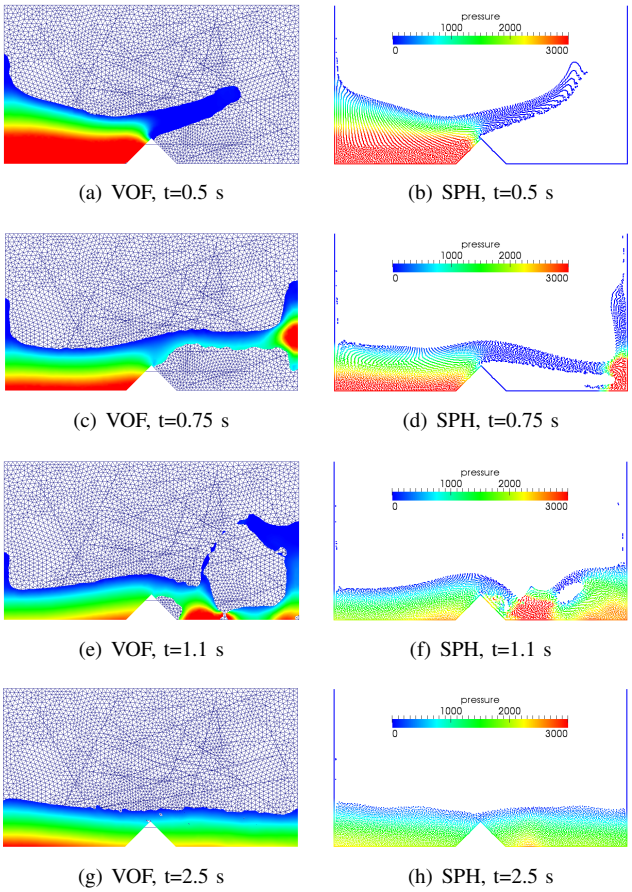

(a) VOF, t=0.5 s (b) SPH, t=0.5 s

(c) VOF, t=0.75 s (d) SPH, t=0.75 s

(e) VOF, t=1.1 s (f) SPH, t=1.1 s

(g) VOF, t=2.5 s (h) SPH, t=2.5 s

Fig. 7. Comparison between VOF and SPH.

In order to study a more complex free-surface flow the dam-break over a wedge will be simulated as done before in [1]. Again the force will be calculated as the integral of the pressure along the left wedge wall. A Volume of Fluid simulation is taken as reference solution (OpenFoam [10]). Though, it should be noted that the later is a multiphase simulation and thus some discrepancies are to be expected when compared to the SPH single-phase simulation as illustrated in Fig. 7. As shown, the traditional boundary conditions using fictitious particles or the Leonard-Jones potential fail in predicting the force. Comparing the approach by Ferrand *et al.* [1] with the present one, it can be seen that the volume diffusion term successfully reduces the numerical noise, while still showing the same force profile as shown in Fig. 8.

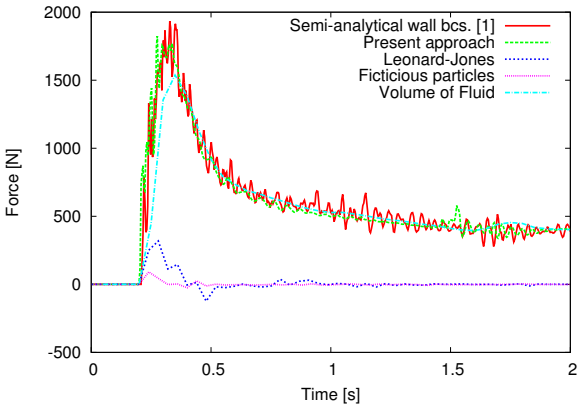

Fig. 8. Comparison of forces on left wedge wall.

VI. Extension to 3-D

In order to extend the formulation presented above to 3-D two major obstacles need to be overcome. Firstly, the mass of a vertex particle needs to be calculated based on the geometry. Secondly, the gradient of γ needs to be evaluated with high accuracy on a boundary element.

Boundary elements in 2-D were line segments and in 3-D they become triangles belonging to a mesh. This is due to the fact that all points on a triangle are coplanar and triangles allow the approximation of arbitrary shapes easily. Explaining the algorithms in detail would go beyond the scope of this paper so a snapshot (Fig. 10) from the simulation of the second SPHERIC test case will provide a preview of the ongoing development.

The 3-D extension required the creation of a preprocessing

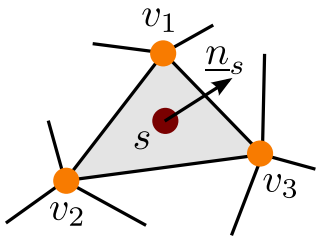

Fig. 9. Vertex particles and boundary segments in 3-D.

software which is called Crixus, developed within this work. The basic workflow uses the SALOME platform [11] to create the triangulated skin-mesh with a specified discretization and afterwards Crixus in order to set the fluid particles as well as initialize the boundaries. Crixus is written in CUDA to allow an efficient execution.

In order to initialize the boundaries, the boundary segments need to be placed and their surface needs to be calculated. The position is chosen to be the centroid of the triangle as illustrated in Fig. 9. However, calculating the mass of the vertex particles is more difficult. The general volume of a fluid

particle is initially represented by a cube with sidelength Δr. The same is true for the vertex particles. However, due to the unstructured nature of the triangle skin-mesh, these volumes will overlap. Additionally, the part of the volume which is not contained in Ω needs to be eliminated. These points are treated using geometrical algorithms and a final numerical integration is used to determine the volume and with that the mass.

The algorithm to calculate $\underline{\nabla}\gamma_{as}$ as given by Eq. (6) is particularly delicate. The first approach was to use a simple second-order integration scheme on a triangle to integrate w on a boundary segment s. If the grid is structured, then this approach works due to the fact that the error is the same on every part of the boundary. As soon as an unstructured grid is used, the error varies along the wall. This causes fluid particles, which slide along a wall, to have values of γ greater than one. In a next step, a 19th-order Gaussian quadrature rule was used as given by [12]. As the integration concerns a non-polynomial function with compact support, using a method tuned towards the integration of polynomials on the entire triangle will yield large errors. Recently, it was possible to find an analytical solution to a special case of the integration over a triangle. This special case can be used to reconstruct the integration of an arbitrary triangle – sphere intersection. This is still work in progress.

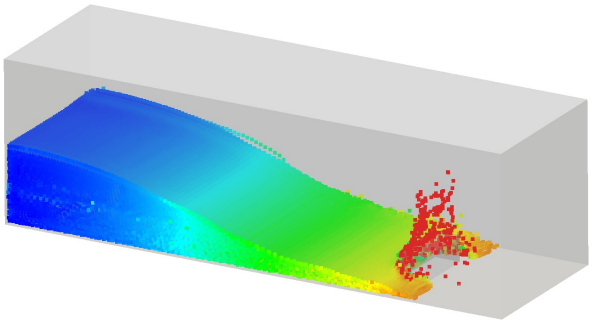

Fig. 10. Snapshot of the SPHERIC 2 test case.

VII. Conclusion

In this paper the basics of the semi-analytical wall boundary conditions by Ferrand *et al.* [1] were revised and then analyzed in a continuous setting, where emphasis was put on the property of skew-adjointness. In order to stabilize the scheme a volume diffusion term introduced by Ferrari *et al.* [2] was reinterpreted in the framework of Reynolds averaged turbulent flows. A modification to this term was proposed in order to avoid unphysical behaviour in case of free-surface flows. The theoretical part is concluded by demonstrating a way of imposing Robin boundary conditions of arbitrary order on a wall.

The next section shows several confined and free-surface flows in order to illustrate the theoretical concepts presented. The laminar Poiseuille flow showed that there is a significant decrease in the order of convergence if a time-dependent continuity equation is used. This fact certainly demands further research to find the cause of this behaviour. The first still water test case shows an infinite open channel in order to illustrate the impact of the proposed correction in the volume diffusion term. The second one, demonstrates the Neumann boundary conditions presented in Section IV. Next follows a simulation of a standing wave in a periodic channel showing the capabilities of the theoretical constructs and highlighting the difficulties in this test case. Finally, a dam break over a wedge is simulated. The force on the left wedge wall is compared to other traditional boundary conditions, which fail to reproduce the Volume of Fluids reference solution. The boundary conditions by Ferrand *et al.* [1] show a slightly more oscillatory signal than the method proposed herein.

Finally this paper is concluded by giving a short overview over the challenges associated to the extension to 3-D. The proposed algorithms are briefly described and a preliminary simulation is shown.

Acknowledgment

The authors would like to thank Dominique Laurence for the constructive conversations and Christophe Kassiotis for providing the Volume of Fluids simulations.

References

[1] M. Ferrand, D. Laurence, B. D. Rogers, D. Violeau, and C. Kassiotis, "Unified semi-analytical wall boundary conditions for inviscid, laminar or turbulent flows in the meshless SPH method," *International Journal for Numerical Methods in Fluids*, 2012.

[2] A. Ferrari, M. Dumbser, E. F. Toro, and A. Armanini, "A new 3D parallel SPH scheme for free surface flows," *Computers & Fluids*, vol. 38, no. 6, pp. 1203–1217, Jun. 2009.

[3] M. Ferrand, D. Laurence, B. D. Rogers, and D. Violeau, "Improved time scheme integration approach for dealing with semi analytical boundary conditions in SPARTACUS2D," in *Proceedings of the 5th International SPHERIC Workshop*, Manchester, Jun. 2010, pp. 98–105.

[4] M. Ferrand, D. Violeau, B. D. Rogers, and D. Laurence, "Consistent wall boundary treatment for laminar and turbulent flows in SPH," in *Proceedings of the 6th SPHERIC Workshop*, Hamburg, Jun. 2011, pp. 273–282.

[5] D. Violeau, *Fluid Mechanics and the SPH Method: Theory and Applications*. Oxford University Press, May 2012, in Print. [Online]. Available: http://ukcatalogue.oup.com/product/academic/earthsciences/hydrology/9780199655526.do

[6] S. Kulasegaram, J. Bonet, R. W. Lewis, and M. Profit, "A variational formulation based contact algorithm for rigid boundaries in two-dimensional SPH applications," *Computational Mechanics*, vol. 33, no. 4, pp. 316–325, Mar. 2004.

[7] J. P. Morris, P. J. Fox, and Y. Zhu, "Modeling low reynolds number incompressible flows using SPH," *Journal of Computational Physics*, vol. 136, no. 1, pp. 214–226, Sep. 1997. [Online]. Available: http://www.sciencedirect.com/science/article/pii/S0021999197957764

[8] M. Basa, N. J. Quinlan, and M. Lastiwka, "Robustness and accuracy of SPH formulations for viscous flow," *International Journal for Numerical Methods in Fluids*, vol. 60, no. 10, pp. 1127–1148, 2009. [Online]. Available: http://dx.doi.org/10.1002/fld.1927

[9] R. G. Dean and R. A. Dalrymple, *Water Wave Mechanics for Engineers & Scientists (Advanced Series on Ocean Engineering-Vol2)*. World Scientific Publishing Company, Jan. 1991.

[10] "OpenFOAM," 2012. [Online]. Available: www.openfoam.org

[11] "SALOME," 2012. [Online]. Available: www.salome-platform.org

[12] D. A. Dunavant, "High degree efficient symmetrical gaussian quadrature rules for the triangle," *International Journal for Numerical Methods in Engineering*, vol. 21, no. 6, p. 11291148, 1985. [Online]. Available: http://dx.doi.org/10.1002/nme.1620210612